Structure, Vol. 12, 2249–2256, December, 2004, ©2004 Elsevier Ltd. All rights reserved. DOI 10.1016/j.str.2004.10.008

Structure of a Xanthine Oxidase-Related 4-Hydroxybenzoyl-CoA Reductase with an Additional [4Fe-4S] Cluster and an Inverted Electron Flow

Mihaela Unciuleac,[1] Eberhard Warkentin,[2] Christopher C. Page,[3] Matthias Boll,[1,*] and Ulrich Ermler[2,*]
[1]Institut für Biologie II
Mikrobiologie Schänzlestrasse 1
D-79104 Freiburg
[2]Max-Planck-Institut für Biophysik
Marie-Curie-Strasse 15
D-60439 Frankfurt
Germany
[3]The Johnson Research Foundation and
Department of Biochemistry and Biophysics
University of Pennsylvania
Philadelphia, Pennsylvania 19104

Summary

The Mo-flavo-Fe/S-dependent heterohexameric protein complex 4-hydroxybenzoyl-CoA reductase (4-HBCR, dehydroxylating) is a central enzyme of the anaerobic degradation of phenolic compounds and belongs to the xanthine oxidase (XO) family of molybdenum enzymes. Its X-ray structure was established at 1.6 Å resolution. The most pronounced difference between 4-HBCR and other structurally characterized members of the XO family is the insertion of 40 amino acids within the β subunit, which carries an additional [4Fe-4S] cluster at a distance of 16.5 Å to the isoalloxazine ring of FAD. The architecture of 4-HBCR and concomitantly performed electron transfer rate calculations suggest an inverted electron transfer chain from the donor ferredoxin via the [4Fe-4S] cluster to the Mo over a distance of 55 Å. The binding site of 4-hydroxybenzoyl-CoA is located in an 18 Å long channel lined up by several aromatic side chains around the aromatic moiety, which are proposed to shield and stabilize the postulated radical intermediates during catalysis.

Introduction

Aromatic compounds serve as important growth substrates for numerous aerobic and anaerobic bacteria (for recent reviews, see Schink et al., 2000; Boll et al., 2002; Gibson and Harwood, 2002). Under anoxic conditions, all oxygen-dependent reactions (ring hydroxylation or cleavage catalyzed by mono- or dioxygenases) are replaced by alternative processes. The dehydroxylation of the phenolic functionality has exclusively been found in the aromatic metabolism of anaerobic bacteria. It plays an important role in the anaerobic biodegradation of low molecular aromatic products derived from lignin decomposition. The only phenolic ring dehydroxylating enzyme studied so far is 4-hydroxybenzoyl-CoA reductase from *Thauera aromatica* (for review, see Boll, 2004) (Figure 1).

*Correspondence: ulrich.ermler@mpibp-frankfurt.mpg.de (U.E.), boll@biologie.uni-freiburg.de (M.B.)

The 275 kDa enzyme consists of three subunits with 82, 35, and 17 kDa, suggesting an $(\alpha\beta\gamma)_2$ composition (Brackmann and Fuchs, 1993; Breese and Fuchs, 1998). A low-potential ferredoxin serves as in vivo electron donor for the enzyme (Breese and Fuchs, 1998; Boll and Fuchs, 1998). Based on the metal content and on EPR and Mößbauer spectroscopic studies, the enzyme was suggested to contain two $[2Fe\text{-}2S]^{+1/+2}$, one $[4Fe\text{-}4S]^{+1/+2}$, one FAD, and one Mo cofactor per monomer (Boll et al., 2001). The genes coding for the three subunits of 4-HBCR were sequenced in *Rhodopseudomonas palustris* (Gibson et al., 1997) and *T. aromatica* (Boll et al., 2001) with 47%–62% amino acid sequence identity. Furthermore, in the genome of the magnetotactic *Magnetospirillum magnetotacticum*, homologous sequences to the three structural genes of 4-HBCR from *T. aromatica* were identified (70%–91% amino acid similarities) (Boll, 2004).

The amino acid sequences of the three subunits of 4-HBCR show significant similarities to enzymes of the xanthine oxidase (XO) family (20%–35% identity) and to aerobic CO dehydrogenase (CODH) (Dobbek et al., 2002). Structurally characterized members of these enzymes comprise aldehyde oxidoreductase from *Desulfovibrio gigas* (Romão et al., 1995), XO from bovine (Enroth et al., 2000) and *Rhodobacter capsulatus* (Truglio et al., 2002), as well as CO dehydrogenase from *Oligotropha carboxidovorans* (Dobbek et al., 2002) and *Hydrogenophaga pseudoflava* (Hanzelmann et al., 2000). 4-HBCR is inactivated by cyanide, which is a typical feature of xanthine-oxidase-family enzymes (Brackmann and Fuchs, 1993). Cyanide reacts with Mo-coordinated inorganic sulfur atom, yielding thiocyanate and inactivated desulfo-enzyme (for reviews, see Hille, 2002; Schindelin et al., 2001; Lowe, 2002).

In spite of the high similarities to members of the XO family and CODH, some features of 4-HBCR are unique: (1) the β subunit harbors a domain consisting of approximately 40 amino acids with five conserved cysteine residues. This domain was suggested to be involved in coordinating a $[4Fe\text{-}4S]^{+1/+2}$ cluster (Breese and Fuchs, 1998). (2) The redox potentials of the FAD·/FADH and Mo(V)/(IV) transitions are exceptionally low (Equation 1). (3) 4-HBCR is the only member of the XO family whose function is to catalyze the reduction of the substrate, suggesting an inverted electron flow. Although XO can reduce uric acid to xanthine to a small amount in the presence of dithionite, this activity is not considered to play a functional role. Notably, 4-HBCR fails to catalyze the hydroxylation of benzoyl-CoA in the presence of oxidized one-electron acceptors with redox potentials >0 mV (unpublished data). (4) The mechanism of reductive removal of a hydroxyl group is not considered to represent a reversal of the reaction sequence of molybdenum hydroxylases. For members of the XO family, evidence for a two-electron rather than a one-electron chemistry of substrate hydroxylation has been reported (Stockert et al., 2002). In contrast, a Birch-like one-electron reduction mechanism by means of highly reactive

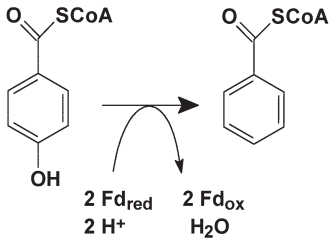

Figure 1. Reaction Catalyzed by 4-Hydroxybenzoyl-CoA Reductase

radical intermediates has been proposed for enzymatic dehydroxylation of the phenol ring (Brackmann and Fuchs, 1993; Boll et al., 2001; Buckel and Keese, 1995). Although experimental evidence for this proposal is still lacking, alternative scenarios appear to be energetically less favorable. (5) 4-HBCR is the only XO family enzyme with a coenzyme A thiol ester substrate, suggesting additional binding sites for the exceptionally large substrate. The thiol ester functionality is supposed to play an essential role in stabilizing substrate radical intermediates.

In this work, 4-HBCR was structurally characterized at 1.6 Å resolution. Using the molecular coordinates, the electron transfer rates between the individual redox centers were calculated. Despite similarities to other XO enzymes, several unique structural features of 4-HBCR provide insights into how an enzyme of the molybdenum-containing hydroxylase type is converted into a dehydroxylase with an inverted electron flow and a proposed differing mechanism of catalysis.

Results and Discussion

Overall Structure

The structure of 4-HBCR established at 1.6 Å resolution (Table 1) revealed the same butterfly-shaped overall architecture as the other structurally characterized members of the XO family (Dobbek et al., 2002; Romão et al., 1995; Truglio et al., 2002; Hanzelmann et al., 2000) (Figure 2). Each $\alpha\beta\gamma$ unit of the heterohexameric 4-HBCR is endowed with a complete set of redox centers and an active site; each $\alpha\beta\gamma$ unit is proposed to function independently. Substantial global differences, in particular between 4-HBCR and the structurally characterized oxidizing enzymes of the XO family, are observed in the relative arrangement of the two $\alpha\beta\gamma$ units within the protein complex. Compared to XO (Enroth et al., 2000; Truglio et al., 2002) and CODH (Dobbek et al., 2002; Hanzelmann et al., 2000), the angle between the two $\alpha\beta\gamma$ units is reduced by about 25° (versus XO). The more closed state leads to an additional interface between two subunits γ of the $(\alpha\beta\gamma)_2$ heterohexamer; the buried surface area being 250 Å^2. In particular, one hydrogen bond is formed between the side chain of Lysγ2 and the carbonyl oxygen of Gluγ'15 and vice versa.

The Subunits of 4-HBCR and the Binding Mode of Their Redox Cofactors

Subunit α (α9–α769) carrying the molybdopterin cofactor is built up of three closely attached domains arranged in a heart-like shape similar to other Mo enzymes of the XO family. The rmsds between subunit α and the equivalent modules of CODH from *O. carboxidovorans* and bovine XO are both 2.2 Å, taking into account 85% of the C_α atoms (Holm and Sander, 1993).

In 4-HBCR, the molybdopterin cofactor was found as molybdenum cytosine dinucleotide and not as molybdopterin mononucleotide, as proposed from a previous biochemical analysis (Brackmann and Fuchs, 1993). This finding suggests that the Mo cofactor from 4-HBCR is labile to the common analysis procedure of molybdopterin cofactors. The conformation of the pterin cofactor of 4-HBCR corresponds to that of CODH except for the ribose conformation, which is C3′ and C2′ endo and not C3′ and C2′ exo (Dobbek et al., 2002). The typical bent conformation between the bicyclic pterin and a monocyclic pyran ring of about 70° is also found in 4-HBCR. Due to the high resolution, the ligation of the redox-active molybdenum could be accurately analyzed (Figure 3). Two coordinating oxo and one hydroxyl ligand were clearly identified, showing distances to the molybdenum of 2.0 Å, 2.0 Å, and 2.2 Å, respectively. Together with the two dithiolene sulfurs, they form a distorted square pyramidal coordination geometry around the central atom (Figure 3). This molybdenum coordination is conserved within the XO family and agrees with the assumption that under the crystallization conditions of 4-HBCR, molybdenum is present in the VI state. A molecular explanation for the very low redox potential of the Mo(IV)/Mo(V) couple (Equation 1) cannot be derived. In contrast to the structure based on crystals soaked with cyanide (data set 2b), the structure without cyanide treatment (based on data set 2a) revealed, in addition to the ligands mentioned above, an electron density peak (termed "X") trans to the apicial Mo = O position. This peak has a distance of about 2.3 Å from the molybdenum (Figure 3) and would be consistent with an oxygen or a sulfur atom with occupancies of 40% and 20%, respectively. Although it is well known that 4-HBCR has a -SH ligand in its active form and is inactivated by cyanide (Boll et al., 2001), an assignment of X as a trans-positioned, cyanolysable sulfur ligand is not justified, as it would not be in line with basic molybdenum complex chemistry, and a sulfur atom would substantially overlap with the dithiolene sulfurs (2.7 Å apart). Additionally, the apparent close distance of X to the oxygen atom of Gluα726 implies a conformational shift of the carboxyl group in the X-bound state that is not visible in the electron density map.

Subunit β (β1–β323) containing one FAD molecule and one [4Fe-4S] cluster differs by an rmsd of about 1.5 Å and 2.3 Å from those of CODH and bovine XO, using 86% and 82% of the C_α atoms for reference (Holm and Sander, 1993), respectively. Subunit β exhibits a FAD binding motif typical for the vanillyl-alcohol oxidase family (Fraaije et al., 1998), which is conserved within the XO family. The polypeptide surrounding of the isoalloxazine ring is significantly modified within the XO family. The loop between Argβ226 and Leuβ235, only found in CODH and 4-HBCR, contacts the N^5 atom via the carbonyl oxygen of Valβ231. Moreover, only 4-HBCR contains an arginine (Argβ121) and phenylalanine (Pheβ233) forming an amino-aromatic interaction at the *si*-side of

Table 1. Crystallographic and Refinement Data of 4-HBCR from *Thauera aromatica*

Crystal form	1	2	
Crystal		a	b
Space group	$P2_12_12_1$	$P2_12_12_1$	$P2_12_12_1$
a (Å)	116.6	112.9	113.0
b (Å)	150.2	152.3	151.8
c (Å)	175.3	174.6	174.9
No. of molecules/asymmetric unit	1	1	1
Solvent content (%)	57	58	58
Resolution (Å)	2.2 (2.28–2.2)	1.7 (1.8–1.7)	1.6 (1.8–1.6)
R_{sym} (%)	5.8 (23)	8.1 (33)	6.3 (17.4)
I/σ	19.2 (3.5)	13.2 (2.3)	17.5 (4.5)
Completeness (%)	95.7 (87.9)	97.0 (93.6)	86.4 (61)
No. of reflections	149,240	318,643	338,357
Multiplicity	2.6	3.1	2.5
Solution method	MR	MR	MR
R_{cryst} (%)	17.0 (22.7)	17.4 (22.9)	15.1 (19.1)
R_{free} (%)	20.4 (27.9)	20.1 (26.1)	17.3 (22.3)
Sigmaa coordinate error (Å)	0.21	0.15	0.09
Rmsd bonds (Å)	0.012	0.012	0.014
Rmsd angles (°)	1.64	1.68	1.80
Average B (Å^2)	33.8	21.8	18.8
Residues per assym. unit	2 × 1241	2 × 1241	2 × 1241
Ligands per assym. unit	2 × (1 Fe_4S_4, 2 Fe_2S_2, 1 FAD, 1 PCD)[a]		
		4 HEPES	4 HEPES
No. of water molecules	1059	1711	2132
Ions	—	2 Cl^-	2 Cl^-
Total no. of atoms	20,044	20,758	21,179
Ramachandran disallowed angles	6	6	6

All data are measured at cryogenic conditions. R_{sym}, I/σ, and completeness for the last resolution shell are given in parentheses.
[a] PCD = (molybdopterin-cytosine-dinucleotide-S,S)-dioxoaqua-molybdenum(V).

FAD and a polypeptide segment described in the following section. The unique interactions with the flavin cofactor are considered to cause the exceptionally low potential of the FADH·/$FADH_2$ couple in 4-HBCR (Equation 1) (Boll et al., 2001).

The most striking difference between 4-HBCR and the other structures of the XO family is the insertion of a 41-residue-long polypeptide segment (Thrβ118–Thrβ158) positioned close to the *si*-face of FAD, partially replacing the NAD binding site in xanthine dehydrogenase (Figure 4). This insertion segment can be subdivided in an irregular region that carries the [4Fe-4S] cluster and a small helical region (β124–β137) that connects the solvent-exposed insertion segment with subunits α and β. Notably, the interface between the helical segment and subunit α is characterized by several interactions involving arginines and tryptophanes. Trpβ130Nε1 of the insertion segment is hydrogen bonded to Arg46O of subunit α, Trp231O to Arg101Nε1, and Trp231Nε1 to Met686O. Interestingly, Thrβ297 involved in fixing the insertion segment is only about 15 Å apart from the contact area between the two subunits γ. This area might indirectly be involved in the stabilization of the insertion region (Figure 2). The average temperature factor of this unique

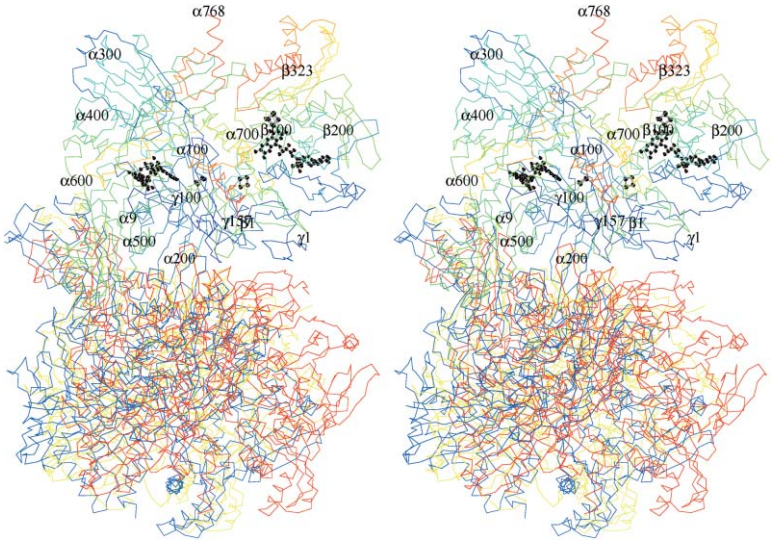

Figure 2. Structure of 4-HBCR from *T. aromatica*

The upper part shows one αβγ trimer with the line color changing from blue to red along the sequence. The lower part shows the respective second trimer of 4-HBCR (red), CODH from *O. carboxidovorans* (blue), and bovine XO (yellow) after aligning of the α subunits of the first subunit. 4-HBCR is present in a more closed state, and CODH and XO are present in a more open state. In 4-HBCR, the dimer contacts between the αβγ units are formed between the α and γ subunits, whereas in other XO members they are solely formed by the large α subunit. The cofactors are drawn as ball-and-stick models.

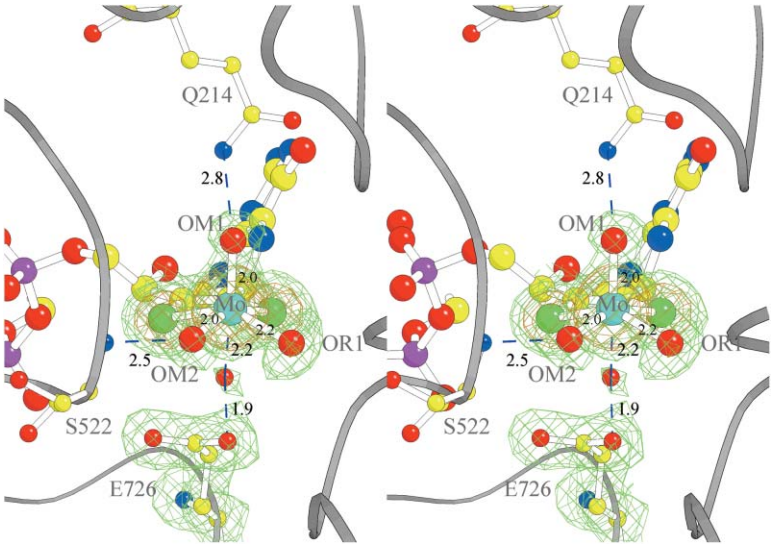

Figure 3. The Ligation of the Molybdenum Atom and the Corresponding Electron Density Based on Crystals Untreated with Cyanide

The electron density at a contour level of 1.2 σ is shown in green, and that of 5 σ is shown in brown. Molybdenum is coordinated by the two thiolene sulfurs, two oxo, and one hydroxy group. Additionally, an extra electron density was observed between the molybdenum and Gluα726 (site "X").

insertion segment of 16.5 Å^2 is in reasonable agreement with the overall average value of 18.8 Å^2.

The low-potential [4Fe-4S] cluster seems to be present in two conformations with a relative shift of 0.4 to 0.7 Å or in one position with a very anisotropic temperature factor. Surprisingly, this displacement leaves the structure of the surrounding residues almost unaffected. The cluster is coordinated to Cysβ122, Cysβ138, Cysβ146, and Cysβ155 with distances of about 2.3 Å between the sulfhydryl sulfurs and the iron atoms (Figure 4). The environment of the cluster is highly hydrophobic, as documented by the side chains of Pheβ124, Lysβ124, Valβ148, and Tyrβ125 within a radius of 4.5 Å. The sole polar contact to the cluster is formed between Tyrβ156NH and a cluster sulfur. The direct cluster surrounding and the redox potential of −465 mV (Equation 1) are comparable to that found in bacterial ferredoxins (Sticht and Rösch, 1998). This system provides a beautiful example of efficient design of a [4Fe-4S] cluster binding site. Only 25 amino acids (without the helical segment) are necessary for adjusting four cysteine side chains for optimal cluster ligation and for wrapping the entire cluster to shield it from the bulk solvent (Figure 4). However, the interactions between the helical segment and subunits α and β substantially stabilize the insertion segment.

Subunit γ (γ1–γ157), harboring two [2Fe-2S] clusters, is the most conserved in the entire XO family, with an rmsd of 1.1 Å and 1.7 Å relative to CODH and bovine XO, respectively (Holm and Sander, 1993). Consequently, the binding modes of the [2Fe-2S] clusters I and II are well conserved among XO enzymes, reflecting the highly similar redox potentials (Equation 1).

The Function of the [4Fe-4S] Cluster in the Electron Transfer Process

The overall reduction of 4-OHBCoA to BCoA and H_2O (E′° is approximately −100 mV for the free acids) (Boll et al., 2001; Thauer et al., 1977) by reduced ferredoxin

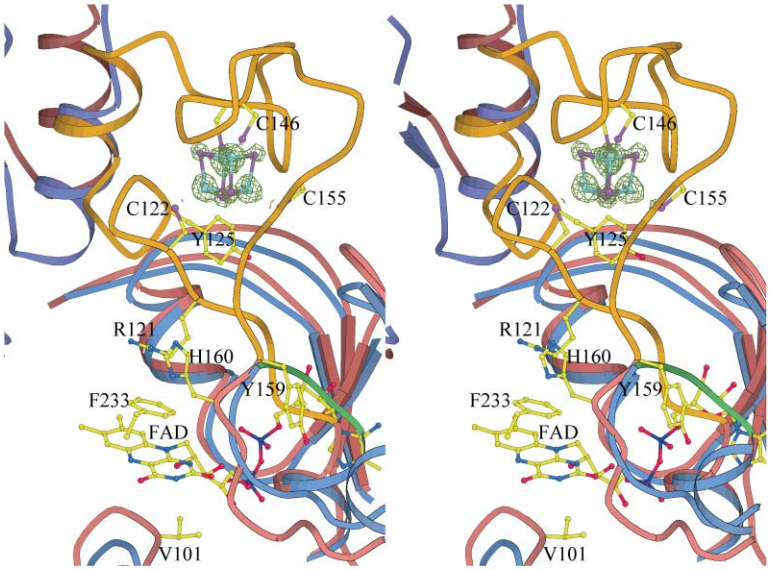

Figure 4. Structure of the Insertion Segment

The insertion segment shown in orange is composed of 40 amino acids from Cysβ118 to Tyrβ158 and wraps the [4Fe-4S] cluster. The distances between the irons and the cysteine sulfurs are between 2.2 and 2.4 Å. The omit density in green is at 5.5 σ level. The hypothetical split positions are indicated by small spheres. The superimposed structures of 4-HBCR and CODH from *Oligotropha carboxidovorans* are shown in red and blue, with the "shortcut" from Ala C117 to Pro C121 shown in green for the latter.

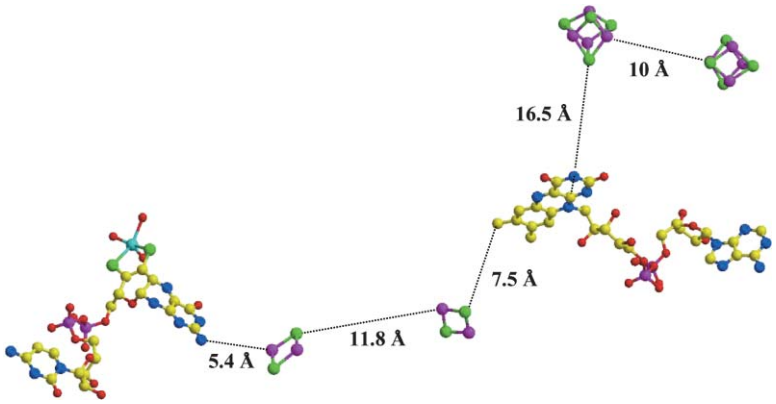

Figure 5. Arrangement of the Cofactors of One $\alpha\beta\gamma$ Unit of 4-HBCR

The atom colors are as follows: Mo, cyan; Fe, magenta; S, green; O, red; N, blue; C, yellow. The electron transfer in the two $\alpha\beta\gamma$ units proceeds independently. Notably, the one- to two-electron carrier FAD lies in the chain between one-electron carriers and most probably fulfills the unusual role as one-electron mediator. In addition, the ferredoxin [4Fe-4S] cluster (above right) is shown in a modeled position.

is considered to be an irreversible process. However, to accomplish reduction of the kinetically inert aromatic substrate at physiological rates, electrons of extremely low potential are required. Therefore, the unusually low redox potential for the Mo(IV)/Mo(V) couple of −500 mV has been suggested as essential for the first electron transfer (Boll et al., 2001). An active role in this process for the extra [4Fe-4S]$^{+1/+2}$ cluster and for FAD is supported by recent EPR and Mössbauer spectroscopic studies, which revealed that the reduced [4Fe-4S]$^{+}$ cluster is oxidized by addition of the substrate (Boll et al., 2001).

Figure 5 shows one [4Fe-4S] cluster of *T. aromatica* ferredoxin (for structure, see Unciuleac et al., 2003) positioned to 4-HBCR at its closest approach to the extra [4Fe-4S] cluster. This creates an essentially linear chain between bound ferredoxin and the molybdenum at the catalytic site of 4-HBCR, with one [4Fe-4S] cluster of the *T. aromatica* ferredoxin at a minimum distance of 10 Å to the 4-HBCR [4Fe-4S] cluster. In contrast, a minimized modeled distance between the ferredoxin [4Fe-4S] cluster and the flavin cofactor is approximately 19 Å. A simple calculation (Page et al., 1999) estimates a difference in tunneling rate between the two cases of $>10^5$-fold, strongly favoring initial electron transfer from ferredoxin to the extra [4Fe-4S] and hence mandating inclusion of the flavin as a linear member of the cofactor chain to the catalytic site. The chain sequence and approximate redox potentials (versus SHE; Boll et al., 2000, 2001) would be as follows:

$$\underset{-585/-435}{Fd_{red}} - \underset{-465}{[4Fe\text{-}4S]} - \underset{-250/-470}{FAD} - \underset{-255}{[2Fe\text{-}2S]\ II} - \underset{-250}{[2Fe\text{-}2S]\ I} - \underset{-380/-500}{Mo\text{-}pterin} - \underset{-100}{4\text{-}HBCoA}\ (mv) \quad (1)$$

In this arrangement, the total distance from the iron-sulfur cluster of substrate ferredoxin to the catalytic molybdenum site is a considerable 55 Å. Electron-tunneling rates between ferredoxin and Mo depend on many factors, but most dominant is the length and nature of the intervening protein. Extensive analysis of many oxidoreductase structures demonstrates that physiological electron transfer (ET) steps rarely are longer than 14 Å edge to edge between the redox cofactors (Page et al., 1999, 2003). Consistent with this, we find that the edge-to-edge distances between the molybdenum cofactor, the two [2Fe-2S]$^{+2/+1}$, and the FAD are conserved within the xanthine oxidase family and fall between 5.4 Å and 11.8 Å (Figure 5). Simple calculations (C.C.P., unpublished data) indicate that electron-tunneling rates in xanthine oxidase are intrinsically faster than measured proton exchanges (Hille and Anderson, 2001) and catalysis, despite unfavorable free energies of individual steps in the cofactor chains. Thus, electron tunneling per se is not rate limiting.

However, in 4-HBCR the distance between the newly described [4Fe-4S] cluster and FAD is 16.5 Å and joins several other exceptions in functional electron transfers that exceed 14 Å (Page et al., 2003). It is then worth examining if the intervening protein medium has evolved in any way to compensate for this long distance. Possibilities include a significantly enhanced intervening protein packing density (Page et al., 1999) or the presence of a covalent bridge to link [4Fe-4S] and FAD. We calculate for this electron transfer a packing density of 0.86, which is one standard deviation higher than the average value of 0.74. This enhancement is equivalent to a 30-fold enhancement in the rate (Page et al., 1999). Closer examination of the structure shows the higher packing density is reflected by an intervening σ-bonded polypeptide from the [4Fe-4S] directed toward the FAD (Figure 4). This includes the Fe ligating Cys 122, several backbone bonds, and then the Arg 121 side chain, followed by Phe233. It is of interest that the amino acids of this structural motif are all conserved in the β subunits of 4-HBCR from *T. aromatica* (Breese and Fuchs, 1998), *R. palustris* (Gibson et al., 1997), and *M. magnetotacticum* (NZ_AAAP01003803.1).

Calculations provide further insights into the function of the additional [4Fe-4S] cluster and test whether it confers unidirectionality to the ET pathway (Page et al., 1999). We find that the inherent tunneling rate from [4Fe-4S]$^{+1}$ to FAD is about 4×10^3 s^{-1}. The actual electron transfer rate will be slowed by coupled events such as proton exchange, measured to be between 3×10^2 and 8×10^3 s^{-1} in XO (Hille and Anderson, 2001), which probably makes this the slowest step of the electron transfer chain in the forward direction. Nevertheless, despite the long distance, the overall ET rate associated through the chain should still be faster than the observed catalytic rate of 1.1×10^2 s^{-1} (Breese and Fuchs, 1998).

The redox potential profile of the electron transfer

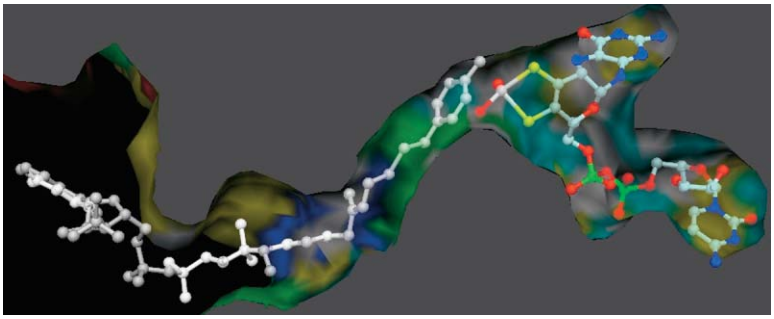

Figure 6. Substrate Binding Site

4-OHBCoA is modeled into a 6 Å wide channel in such a way that the Mo-ligated water is replaced by the hydroxy group of 4-OHBCoA. The benzoyl moiety is flanked by four aromatic residues comprising Tyrα319, Tyrα326, Hisα360, and Tyrα521 (surface colors: blue, basic; red, acidic; cyan, polar; green, aromatic; yellow, aliphatic).

is U shaped (Equation 1): low potential cofactors are positioned at the beginning and at the end of the chain, with the higher potential [2Fe-2S] clusters harbored in between. In the forward direction, tunneling calculations find that the final uphill electron-tunneling steps are not rate limiting due to the short distance between these centers (6.1 Å), provided that the pterin moiety of the molybdenum cofactor is redox active (Romão et al., 1995; Huber et al., 1996). However, in the reverse direction, ET from FADH· to the extra $[4Fe\text{-}4S]^{+2}$ cluster is impeded not only by the putative uphill step but also by the 16.5 Å distance. Thus, the U-shaped free energy profile, which places the uphill step at a long distance for the reverse reaction and a short distance for the forward direction, serves to favor unidirectional ET while maintaining a chain transfer rate faster than catalysis.

Meanwhile, genes have been found in other sequenced microbial genomes coding for unknown enzymes of the XO family with unknown functions containing similar [4Fe-4S] cluster insertion segments to 4-HBCR (Boll, 2004). This finding emphasizes the importance of the additional [4Fe-4S] clusters in XO-like enzymes, and the question arises of whether the insertion segment is typical for enzymes that catalyze reduction processes (perhaps reductive dehydroxylation of other substrates), thereby requiring an inverted electron flow.

Reaction of 4-HBCR

A Birch-like reduction mechanism has been proposed for enzymatic dehydroxylation of 4-OHBCoA with single alternate ET and protonation steps to the aromatic benzoyl ring by means of transient radical intermediates (Brackmann and Fuchs, 1993; Boll et al., 2001; Buckel and Keese, 1995). Such a reaction mechanism clearly differs from the generally assumed two-electron chemistry of substrate oxidation in XO-family enzymes (Stockert et al., 2002). Therefore, it was surprising to find that in 4-HBCR the surrounding of the redox centers and the dithiolene/oxygen ligands of molybdenum appears to be nearly identical to that in CODH and XO.

Substantial differences were found in the binding mode of the aromatic substrate. The substrate binding site is located in an 18 Å long and 6 Å wide channel. Its size is well compatible with the spatial requirements of the bulky 4-OHBCoA (Figure 6) such that no large conformational changes are expected upon substrate binding. Nevertheless, a soaking experiment with the substrate damaged the 4-HBCR crystals; cocrystallization with the nonhydrolyzable 4-hydroxyphenacyl-CoA failed due to poor binding of the analog. Therefore, binding of 4-OHBCoA was modeled, taking into account that in XO-like enzymes the hydroxy group of the substrate replaces a hydroxy/water ligand from the molybdenum. The modeled phenolic ring is surrounded by several aromatic residues including Tyrα319, Tyrα326, Hisα360, and Tyrα521, which are perfectly suited for binding it by van der Waals and probably π-π interactions. The aromatic residues are conserved in 4-HBCR-like proteins but not in the XO family. Moreover, the aromatic residues adjacent to the phenolic ring might stabilize and shield the proposed radical intermediates.

The reaction of 4-HBCR involves a stoichiometric protonation of the substrate (Figure 1). In addition, a proton-assisted ET has been proposed for Birch-like enzymatic reactions, thereby avoiding the generation of highly reactive intermediates (Boll, 2004; Möbitz and Boll, 2002). Potential proton donors would be Gluα726 and Hisα360, which are 3.7 Å and 5.6 Å apart from the hydroxy ligand. The surrounding of Gluα726 is remarkably changed compared to XO and CODH, and the carboxylate group might at least be partly present in the protonated state. Interestingly, upon substrate binding, protons cannot be shuttled from Gluα726 to the bulk solvent; instead, protons can be stored within the hydrogen bond network between Gluα726, Serα523, Gluα723, and Serα725.

Experimental Procedures

Crystallization and Data Collection

4-HBCR was purified (Brackmann and Fuchs, 1993) and crystallized (Unciuleac et al., 2003) under anoxic conditions as described; the specific activity of the purified enzyme was between 11 and 16 μmol 4-HBCoA reduced min^{-1} mg^{-1} and was in the range of the reported values (Brackmann and Fuchs, 1993; Breese and Fuchs, 1998). Two different although similar crystal forms were obtained in the space group $P2_12_12_1$. Diffraction data were collected at the Max-Planck beamline BW6 at DESY in Hamburg (MAD) and at the ESRF beamlines ID14-4 (data sets 1 and 2a) and ID29 (data set 2b) in Grenoble. Data set 2b was measured from a crystal obtained after cocrystallizing the enzyme with 10 mM substrate analog and 1 mM NaCN (Table 1). Data processing and scaling were performed with the HKL suite (Otwinowski and Minor, 1997) (see Table 1).

Phase Determination and Model Building

Phase determination was initiated with the method of multiple anomalous dispersion (MAD). Although the positions of the Fe/S clusters could be located using the program SnB (Weeks and Miller, 1999), the quality of the data was not sufficient for quick progress. In parallel, molecular replacement calculations were performed using the model of CO dehydrogenase (Dobbek et al., 1999) (Protein Data Bank ID code 1QJ2) as the search model. The application of the polyalanine chain of one $\alpha\beta\gamma$ trimer using the program EPMR (Kis-

singer et al., 1999) resulted in correlation coefficients of 0.166 and 0.264 for one and two trimers, respectively. This solution, visualized in O (Jones et al., 1991), revealed the expected butterfly shape of the heterohexamer, a reasonable overall packing, and an agreement with the independently found Fe/S cluster peaks.

Model Refinement and Quality of the Model

Refinement was achieved using CNS (Brünger et al., 1998), applying standard protocols. An initial simulated annealing attempt based on the polyalanine chain (data set 1) resulted in R and R_{free} factors of 0.45 and 0.50, respectively. After an amino acid exchange with the SWISS-PROT server (Guex and Peitsch, 1997) and a subsequent refinement, the R and R_{free} factors dropped to 0.40 and 0.45. At this stage, the calculated electron density was good enough to identify the [4Fe-4S] cluster that was not present in the search model. Model building and refinement was continued using the high-quality data set a of crystal form 2 after a molecular replacement calculation. Finally, the R and R_{free} factors converged to 17.4% and 20.2%, respectively, in the resolution range 20–1.7 Å (see Table 1). The root-mean-square deviation is about 0.3 Å between the two $\alpha\beta\gamma$ units in the asymmetric unit. In contrast to the published sequence (Breese and Fuchs, 1998), the residues 142 to 144 in subunit γ were recognized as lysine, isoleucine, and isoleucine, respectively, and 251 in subunit α as alanine. The electron density at the site of the [4Fe-4S] clusters is poorly matched by the atoms refined with isotropic temperature factors. A better fit causing less residual density was obtained after introduction of a split position. A subsequently performed TLS refinement using REFMAC5 (Murshudov et al., 1997) gave no further clue, as the resulting ellipsoid was not interpretable. The refinement statistics based on three data sets are listed in Table 1. If not explicitely stated otherwise, the interpretation of the structure is based on data set 2b.

Electron Transfer Calculations

ET calculations between the redox centers are based on the following empirical equation (Page et al., 1999): $\log_{10}k_{ex,et} = 13.0 - (1.2 - 0.8\rho)(R - 3.6) - 3.1(\Delta G + \lambda)^2/\lambda$, where $k_{ex,et}$ is the exergonic electron-transferring tunneling rate, the packing density ρ is defined as the volume fraction of atoms to atoms + interstitial space, R is the edge-to-edge distance between the redox centers, ΔG is the free energy, and λ is the reorganization energy that is required to change the nuclear coordinates upon ET.

Preparation of Figures

Figures 2–6 were generated using the programs MOLSCRIPT (Kraulis, 1991), BOBSCRIPT (Esnouf, 1999), RASTER3D (Merritt and Murphy, 1994), MSMS (Sanner et al., 1996), and DINO (Philippsen, www.dino3d.org).

Acknowledgments

This work was supported by the Max-Planck-Gesellschaft, the Deutsche Forschungsgemeinschaft (BO 1565/2-2), and the NIH grant GM41048 to P.L. Dutton. We thank H. Michel (Frankfurt) for continuous support and P.L. Dutton and C.C. Moser (both Philadelphia) for many helpful suggestions. We are grateful to the staff of the BM6 beamline, DESY, Hamburg and the ID14 and ID29 beamlines, ESRF, Grenoble for help during data collection.

Received: March 19, 2004
Revised: October 8, 2004
Accepted: October 13, 2004
Published: December 7, 2004

References

Boll, M., and Fuchs, G. (1998). Identification and characterization of the natural electron donor ferredoxin and of FAb as a possible prosthetic group of benzoyl-CoA reductase (dearomatizing), a key enzyme of anaerobic aromatic metabolism. Eur. J. Biochem. *251*, 946–954.

Boll, M., Fuchs, G., Tilley, G., Armstrong, F.A., and Lowe, D.J. (2000). Unusual spectroscopic and electrochemical properties of the 2 [4Fe-4S] ferredoxin of *Thauera aromatica*. Biochemistry *39*, 4929–4938.

Boll, M., Fuchs, G., Meier, C., Trautwein, A.X., El Kasmi, A., Ragsdale, S.W., Buchanan, G., and Lowe, D.J. (2001). Redox centers of 4-hydroxybenzoyl-CoA reductase, a member of the xanthine oxidase family of molybdenum-containing enzymes. J. Biol. Chem. *276*, 47853–47862.

Boll, M., Fuchs, G., and Heider, J. (2002). Anaerobic oxidation of aromatic compounds and hydrocarbons. Curr. Opin. Chem. Biol. *6*, 604–611.

Boll, M. (2004). Key enzymes in the anaerobic aromatic metabolism catalysing Birch-like reductions. Biochim. Biophys. Acta, in press.

Brackmann, R., and Fuchs, G. (1993). Enzymes of anaerobic metabolism of phenolic compounds. 4-Hydroxybenzoyl-CoA reductase (dehydroxylating) from a denitrifying Pseudomonas species. Eur. J. Biochem. *213*, 563–571.

Breese, K., and Fuchs, G. (1998). 4-hydroxybenzoyl-CoA reductase (dehydroxylating) from the denitrifying bacterium *Thauera aromatica*: prosthetic groups, electron donor, and genes of a member of the molybdenum-flavin-iron-sulfur proteins. Eur. J. Biochem. *251*, 916–923.

Brünger, A., Adams, P.D., Clore, G.M., Delano, W.L., Gros, P., Grosse-Kunstleve, R., Jiang, J.S., Kuszewski, J., Nilges, M., Pannu, N.S., et al. (1998). Crystallography & NMR system: A new software suite for macromolecular structure determination. Acta. Crystallogr. D Biol. Crystallogr. *54*, 905–921.

Buckel, W., and Keese, R. (1995). One-electron redox reactions of coash esters in anaerobic bacteria - a mechanistic proposal. Angew. Chem. Int. Ed. Engl. *34*, 1502–1506.

Dobbek, H., Gremer, L., Meyer, O., and Huber, R. (1999). Crystal structure and mechanism of CO dehydrogenase, a molydo iron-sulfur flavoprotein containing S-selanylcysteine. Proc. Natl. Acad. Sci. USA *96*, 8884–8889.

Dobbek, H., Gremer, L., Kiefersauer, R., Huber, R., and Meyer, O. (2002). Catalysis at a dinuclear [CuSMo(==O)OH] cluster in a CO dehydrogenase resolved at 1.1-angstrom resolution. Proc. Natl. Acad. Sci. USA *99*, 15971–15976.

Enroth, C., Eger, B.T., Okamoto, K., Nishino, T., Nishino, T., and Pai, E.F. (2000). Crystal structures of bovine milk xanthine dehydrogenase and xanthine oxidase: Structure-based mechanism of conversion. Proc. Natl. Acad. Sci. USA *97*, 10723–10728.

Esnouf, R.M. (1999). An extensively modified version of MolScript that includes greatly enhanced coloring capabilities. Acta Crystallogr. D Biol. Crystallogr. *55*, 938–940.

Fraaije, M.W., Van Berkel, W.J., Benen, J.A., Visser, J., and Mattevi, A. (1998). A novel oxidoreductase family sharing a conserved FAD-binding domain. Trends Biochem. Sci. *23*, 206–207.

Gibson, J., and Harwood, C.S. (2002). Metabolic diversity in aromatic compound utilization by anaerobic microbes. Annu. Rev. Microbiol. *56*, 345–369.

Gibson, J., Dispensa, M., and Harwood, C.S. (1997). 4-hydroxybenzoyl coenzyme a reductase (dehydroxylating) is required for anaerobic degradation of 4-hydroxybenzoate by *Rhodopseudomonas palustris* and shares features with molybdenum-containing hydroxylases. J. Bacteriol. *179*, 634–642.

Guex, N., and Peitsch, M.C. (1997). Swiss-model and the swiss-pdb viewer: an environment for comparative protein modeling. Electrophoresis *18*, 2714–2723.

Hanzelmann, P., Dobbek, H., Gremer, L., Huber, R., and Meyer, O. (2000). The effect of intracellular molybdenum in Hydrogenophaga pseudoflava on the crystallographic structure of the seleno-molybdo-iron-sulfur flavoenzyme carbon monoxide dehydrogenase. J. Mol. Biol. *301*, 1221–1235.

Hille, R. (2002). Molybdenum and tungsten in biology. Trends Biochem. Sci. *27*, 360–367.

Hille, R., and Anderson, R.F. (2001). Coupled electron/proton transfer in complex flavoproteins – solvent kinetic isotope effect studies of electron transfer in xanthine oxidase and trimethylamine dehydrogenase. J. Biol. Chem. *276*, 31193–31201.

Holm, L., and Sander, C. (1993). Protein structure comparison by alignment of distance matrices. J. Mol. Biol. *233*, 123–138.

Huber, R., Hof, P., Duarte, R., Moura, J.J.G., Moura, I., LeGall, J., Archer, M., and Romão, M.J. (1996). A structure-based catalytic mechanism for the xanthine oxidase family of molybdenum enzymes. Proc. Natl. Acad. Sci. USA *93*, 8846–8851.

Jones, T.A., Zou, J.Y., Cowan, S.W., and Kjeldgaard, M. (1991). Improved methods for building protein models in electron density maps and the location of errors in these models. Acta Crystallogr. A *47*, 110–119.

Kissinger, C.R., Gehlhaar, D.K., and Fogel, D.B. (1999). Rapid automated molecular replacement by evolutionary search. Acta Crystallogr. D Biol. Crystallogr. *55*, 484–491.

Kraulis, P.J. (1991). MOLSCRIPT: a program to produce both detailed and schematic plots of protein structures. J. Appl. Crystallogr. *24*, 946–950.

Lowe, D.J. (2002). Enzymes of the xanthine oxidase family: The role of molybdenum. Met. Ions Biol. Syst. *39*, 455–479.

Merritt, E.A., and Murphy, M.E.P. (1994). Raster3d version 2.0: a program for photorealistic molecular graphics. Acta Crystallogr. D Biol. Crystallogr. *50*, 869–873.

Möbitz, H., and Boll, M. (2002). A birch-like mechanism in enzymatic benzoyl-CoA reduction: a kinetic study of substrate analogues combined with an ab initio model. Biochemistry *41*, 1752–1758.

Murshudov, G.D., Vagin, A.A., and Dodson, E.J. (1997). Refinement of macromolecular structures by the maximum-likelihood method. Acta Crystallogr. D Biol. Crystallogr. *53*, 240–255.

Otwinowski, Z., and Minor, W. (1997). Processing of X-ray diffraction data collected in oscillation mode. Methods Enzymol. *276*, 307–326.

Page, C.C., Moser, C.C., Chen, X., and Dutton, P.L. (1999). Natural engineering principles of electron tunneling in biological oxidation-reduction. Nature *402*, 47–52.

Page, C.C., Moser, C.C., and Dutton, P.L. (2003). Mechanism for electron transfer within and between proteins. Curr. Opin. Chem. Biol. *5*, 551–556.

Romão, M.J., Archer, M., Moura, I., Moura, J.J.G., Legall, J., Engh, R., Schneider, M., Hof, P., and Huber, R. (1995). Crystal structure of the xanthine oxidase-related aldehyde oxido-reductase from *D. gigas*. Science *270*, 1170–1176.

Sanner, M.F., Spehner, J.-C., and Olson, A.J. (1996). Reduced surface – an efficient way to compute molecular surfaces. Biopolymers *38*, 305–320.

Schindelin, H., Kisker, C., and Rajagopalan, K.V. (2001). Molybdopterin from molybdenum and tungsten enzymes. Adv. Protein Chem. *58*, 47–94.

Schink, B., Philipp, B., and Müller, J. (2000). Anaerobic degradation of phenolic compounds. Naturwissenschaften *87*, 12–23.

Sticht, H., and Rösch, P. (1998). The structure of iron-sulfur proteins. Prog. Biophys. Mol. Biol. *70*, 95–136.

Stockert, A.L., Shinde, S.S., Anderson, R.F., and Hille, R. (2002). The reaction mechanism of xanthine oxidase: evidence for two-electron chemistry rather than sequential one-electron steps. J. Am. Chem. Soc. *124*, 14554–14555.

Truglio, J.J., Theis, K., Leimkühler, S., Rappa, R., Rajagopalan, K.V., and Kisker, C. (2002). Crystal structure of the active and alloxanthine-inhibited forms of xanthine dehydrogenase from *Rhodobacter capsulatus*. Structure *10*, 115–125.

Thauer, R.K., Jungermann, K., and Decker, K. (1977). Energy conservation in chemotrophic anaerobic bacteria. Bacteriol. Rev. *41*, 100–180.

Unciuleac, M., Boll, M., Warkentin, E., and Ermler, U. (2003). Crystallization of 4-hydroxybenzoyl-CoA reductase and the structure of its electron donor ferredoxin. Acta Crystallogr. D Biol. Crystallogr. *60*, 388–391.

Weeks, C.M., and Miller, R. (1999). The design and implementation of SnB version 2.0. J. Appl. Crystallogr. *32*, 120–124.

Accession Numbers

The atomic coordinates for 4-hydroxybenzoyl-CoA reductase have been deposited in the Protein Data Bank with the accession codes 1SB3 for the native structure and 1RM6 for the structure treated with NaCN.